An Inference Based Study of Neutrino Flavor Oscillation

Lizzy Jones
American Museum of Natural History, Harvey Mudd College
Mentor: Eve Armstrong

Abstract

The solar property of electron number density has important implications for understanding solar and stellar physics, yet its precise distribution within the Sun is unknown. While current models are derived from measurements at the solar surface, it would be novel to use Earth-based measurements to predict electron distribution in the Sun. Electron number density dictates the flavor evolution of neutrinos as they stream radially outward from the Sun, and thus determines their flavor when they reach detectors on Earth. In this paper, we explore an inference-based approach that uses neutrino flavor measurements from Earth-bound detectors to extrapolate the Sun's electron density function. We are currently studying logistic and exponential forms of electron number density and ultimately seek the sparsest amount of data required to place useful constraints on the model.

1 Introduction

Electrons exist at the core of many stellar processes, and their distribution within the sun has important implications in solar and stellar physics as well as neutrino physics. However, the precise profile of electron number density is not known because current technology is not capable of probing measurements inside the Sun's core. Solar neutrinos offer an interesting solution to this problem because they are capable of transmitting information to the Earth through high density regions like the Sun.

Neutrinos are created within the sun as a byproduct of nuclear fusion. As they stream outward, the property of neutrino"flavor" determines how they interact with the surrounding matter. There exist three different of neutrino flavors– electron, muon, and tau– and as neutrinos travel and interact with matter, they oscillate between these three flavors [1]. These oscillations are highly nonlinear: not only does the nature and density of the surrounding matter affect a neutrino's flavor, but conversely its flavor affects how it interacts with matter.

Though there are many types of matter particles in the solar core, electrons are the driving factor for neutrino flavor evolution. The electron number density function thus determines the neutrino flavor evolution profile as neutrinos travel through the Sun. Historically, solutions for flavor evolution were found using forward integration, which entails choosing initial conditions of flavor within the Sun's core [2–9]. It has been shown that relaxing these initial conditions only a small amount can have dramatic influences on the solution [10, 11]. Our study investigates an inference-based method to find solutions which does not require knowledge of initial conditions. This model uses optimization to perform parameter estimation and determine a solution based on both a theoretical model and given measurements.

The specific procedure we are using is called Statistical Data Assimilation (SDA). It is a method used in a wide array of applications to combine theoretical models with sparse physical measurements. SDA was developed in the fields of weather prediction and later developed in neurobiology [12–16]. Its capabilities are well-suited for our scenario, which incorporates both a mathematical model of flavor evolution as well as flavor measurements from earth-based detectors. To date, we have applied SDA to a solar model and identified state variable predictions that are consistent with both model and measurements [17–19].

Though we are currently working with solar neutrinos, the ultimate goal of this project is to study to flavor evolution of neutrinos emitted in core-collapse supernovae (CCSN). The presence of neutrinos in CCSN is driven by the reaction $\nu_e + n \rightarrow p + e^-$. The limiting factor for this reaction is ν_e, and therefore the quantity ν_e determines the proton to neutron ratio inside the CCSN. If the proton to neutron ratio is sufficiently low, this indicates that the CCSN environment is potentially capable of forming heavy elements.

By studying the flavor evolution of neutrinos and thereby determining the number of ν_e inside a CCSN, our project seeks to discover the proton to neutron ratio and answer the question about heavy elements. However, neutrino data from CCSN is exceedingly sparse: though it is estimated that approximately 10^{58} neutrinos are emitted per event, only a few dozen were detected from the most recent event, SN1987A [20, 21].

In this paper, we seek to test our procedure on solar neutrinos, for which is far more data available. By developing our parameter estimation procedure on data from the sun, we aim to be prepared to analyze neutrino data when the next CCSN event occurs.

2 Model

The model is explained in detail in Refs. [17–19]. Here we give a brief overview of the model and refer the reader to these references for further detail. We consider monoenergetic beams of neutrinos streaming radially from the sun and interacting with each other and background particles present in the sun. In this paper, we use three beams each of a different energy. We neglect any effects of back scattering and incorporate only forward scattering into the model. In principle, the background particles consist of all particles that carry the weak charge, including electrons, nuclei, and free nucleons. Of these, only electrons are present in high enough quantities to significantly affect the neutrino flavor evolution. Thus, the distribution of background matter $V(r)$ can be approximated as linearly related to electron density. The exact value for $V(r)$ is given by the Wolfenstein correction to neutrino mass [22]:

$$V(r) = \sqrt{2} G_F N_e(r) \tag{1}$$

where G_F is the Fermi constant. The density of electrons $N_e(r)$ decreases with radial distance r from the sun's core. Simply stated, our goal is to determine the functional form of $N_e(r)$ using as little flavor measurement data as possible.

Our model consists of a two flavor, single angle model with three neutrino beams. The two flavor approximation between ν_e and ν_x is reasonable because mu and tau neutrinos experience identical interactions inside the sun [23]. We use a polarization vector $\vec{P}$ to describe the flavor state of the neutrino beams:

$$\frac{\mathrm{d}\vec{P}}{\mathrm{d}r} = (\omega \vec{B} + V(r)\hat{z}) \times \vec{P}, \tag{2}$$

where $\omega = \delta m^2/(2E)$ is the vacuum oscillation frequency of a neutrino with energy E, δm^2 being the mass-squared difference in vacuum [19]. The unit vector $\vec{B} = \sin(2\theta)\hat{x} - \cos(2\theta)\hat{(z)}$ represents flavor mixing in vacuum, with mixing angle θ. The function $V(r)$ arises from neutrino interactions with the background electrons, and whose functional form is the topic of discussion Section 4.2.

In Refs. [17, 18], an additional term is included in the polarization vector to account for neutrino-neutrino coupling. In the solar environment, the contributions of this term are negligible because the density of neutrinos in the sun is too small.

The polarization vector $\vec{P}$ consists of three elements described as follows:

$$\vec{P} = \begin{bmatrix} Px \\ Py \\ Pz \end{bmatrix} = \begin{bmatrix} \psi_e \psi_x^* + \psi_e^* \psi_x \\ i(\psi_e \psi_x^* - \psi_e^* \psi_x) \\ |\psi_e|^2 + |\psi_x^*|^2 \end{bmatrix}. \tag{3}$$

The P_z component of the neutrino polarization vector denotes the net flavor content of electron flavor minus the superposition of muon and tau flavors. This term is related to the survival probability, P_{survival} by propagating the neutrino beam through the vacuum region between the solar surface ($\odot$ s) and Earth ($\oplus$) as described in Ref. [19]:

$$(1 - \sin^2 2\theta)P_{\odot s,z} - \cos 2\theta \sin 2\theta P_{\odot s,x} = 2P_{\text{survival}} - 1. \tag{4}$$

Equation 4 links the state variable evolution term from Equation 2 to P_{survival}, which can be determined experimentally using neutrino measurements at Earth-based detectors. Though the results presented in this paper continue to use simulated data measurements, we are currently working on implementing this Earth/Sun transformation so that we can use real measurements from detectors in our analysis.

3 Method

3.1 Optimization Formulation

The neutrino flavor evolution problem was traditionally solved using forward integration. Whereas an integration approach involves choosing initial values and stepping forward in time, our approach, Statistical Data Assimilation (SDA) is not contingent on knowing initial values. Instead, it uses an optimization procedure that converge toward a solution at every location simultaneously. Optimization takes place in a space of $N \times D + P$ dimensions, where N is the number of time steps, D is the number of state variables used, and P is the number of unknown parameters. This space is discretized using the Hermite-Simpson method.

Using SDA, we seek to maximize the probability of finding a path $\mathbf{X}$ in the model's state space given observations $\mathbf{Y}$:

$$P(\mathbf{X}|\mathbf{Y}) = \mathbf{e}^{-\mathbf{A_0}(\mathbf{X},\mathbf{Y})}. \tag{5}$$

The procedure begins with a random guess (within the specified search ranges) for each point in the discretized parameter space. We use a cost function A_0 to determine the error of this guess. The cost function takes the form

$$A_0 = R_f A_{\text{model}} + R_m A_{\text{meas}}, \tag{6}$$

where A_{model} and A_{meas} penalize deviation of the guess from the model and measurement respectively. The functional forms of these terms are given in Ref. [19]. Values for R_f and R_m are set to determine the relative weights of the model and measurement error terms. R_m is set to a constant value (for this paper, $R_m = 1$), whereas R_f takes the form $R_{f,0}\alpha^{\beta}$. For this paper, we set $R_f, 0 = 10^{-3}$ and $\alpha = 2.0$. We use the open-source library Interior-point Optimizer (Ipopt) to perform the optimization and minimize the cost function.

3.2 Identifying the Lowest Minimum on the Cost Function

The cost surface is non-convex, so to avoid falling into local minima, the optimization is performed using simulated annealing [24]. The annealing parameter, β, is initialized at zero. In this case, R_f is small so the cost function is dominated by the measurement term. The cost surface for the measurement terms is convex, so the optimization procedure easily finds the global minimum. The value of β is then incremented by 1 to increase the weight of the model term, and the cost function is recalculated. We continue increasing β, and by the time $R_f \gg R_m$ and the cost surface is complex, the goal is that we have already situated ourselves near enough to the global minimum so that the guess does not fall into a local minimum.

4 Experiments

4.1 The Task for Optimization

Our ultimate goal is to use SDA to combine Earth-based measurements with model dynamics and predict the electron number density function within the sun. In practice, we provide the procedure with the full form of $V(r)$ except for a single parameter, for which we provide a search range of possible values. The procedure must estimate this parameter while simultaneously solving for the state variables P_x, P_y, and P_z. To inform the optimization procedure, we provide experimentally detected measurements of neutrino flavor at the solar surface using data from the Borexino experiment [25].

This experimentally-measured $P_{survival}$ value is currently not sufficient information to determine a unique solution. To further constrain the model, we also include simulated "measurements" of flavor near the core of the sun. Our simulated model is generated by specifying the energies of the three neutrino beams based on experimentally detected neutrino energies [25]. We assume each beam is pure ν_e at the solar core so that the initial value of P_z is 1.0. P_x and P_y are initialized at zero. We also provide a value for the single unknown parameter in $V(r)$. Using these constraints, the model is generated by forward integration using 121,901 steps with a step size of $\delta r = 2.85237$.

Measurements of this solution are taken at various locations and are used in the optimization procedure to help constrain possible outcomes. We used different numbers of "measurements" for each experiment as specified in the next section. We also use this model as a source to serve as a comparison for the solution generated by our optimization procedure.

4.2 Forms of $V(r)$

We ran two separate experiments, each with a different functional form of $V(r)$. The first is an exponential decay of the form

$$V(r) = p_c \mathrm{e}^{-\frac{p_a}{p_b} r}. \tag{7}$$

For our experiments, we use the values $p_a = 13$, $p_b = 347703.903$, and $p_c = 0.09477$.

For the exponential model, we provided the procedure with measurements for P_z at every 10-20 locations spaced along the first and last 1000 locations of the full trajectory. Providing measurements at slightly spaced random intervals rather than at every point gives the optimization procedure flexibility and avoids over-fitting.

The second form of this function is a logistic decay:

$$V(r) = \frac{L}{(1 - q\mathrm{e}^{k(r - x_0)})^{\frac{1}{q}}}. \tag{8}$$

In our experiment, we use $L = 4.7 \times 10^2$, $q = 1.7$, $k = 2.7 \times 10^{-5}$, and $x_0 = 7.0 \times 10^4$.

For the logistic model, we gave measurements to the procedure at every 10 to 20 points spaced along the entire P_z trajectory (rather than only the first and last 1000 points, as was used for the exponential model). Again, we choose slightly spaced, random intervals to avoid over-fitting.

5 Results

5.1 Exponential Function for Electron Number Density

Our first experiment uses the exponential form of $V(r)$ as described by Eq. 7. We generated model beams by setting parameters to the values specified above. For the optimization experiment, we provided the procedure with values only for p_b and p_c but not for p_a. Our goal was

to solve for the nine state variables (P_x, P_y, and P_z for each beam) as well as the unknown parameter p_a.

The optimization procedure completed 25 iterations of increasing β (until $\beta = 25$). We applied a search range of $0.01 - 20$ for p_a which was asymmetric about the true value of $p_a = 13$. This asymmetry is critical, as the search procedure has a bias toward the edges and midpoint of the search range. When it fails in parameter estimation, it tends to "flee" to one of these values for the remainder of the iterations.

Our results are shown in Figure 1. Figure 1a shows solutions for the state variables plotted against the corresponding model values for iteration $\beta = 23$. Figure 1b shows the estimated value of p_a for each β iteration.

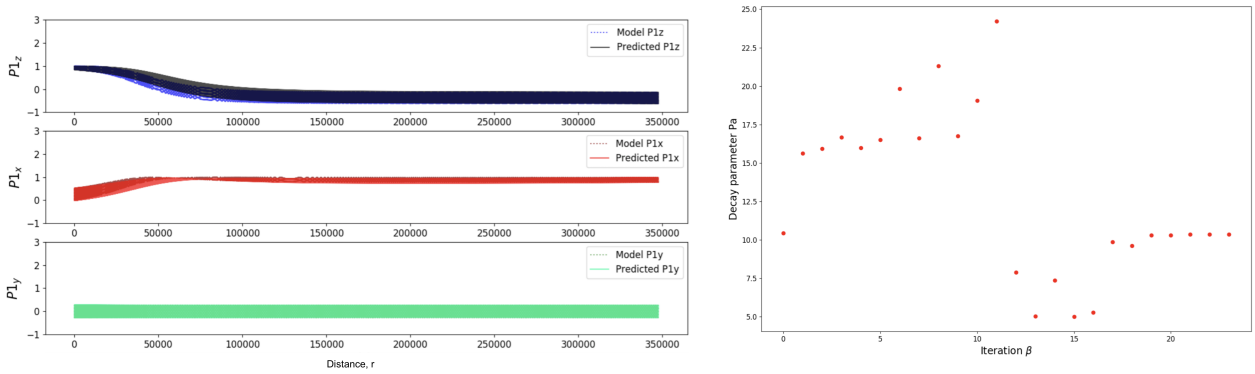

(a) State variable evolution for $\beta = 23$

(b) Estimated parameter value vs. β iteration

Figure 1: Results from the optimization procedure for an exponentially decaying $V(r)$ model

As Fig. 1a illustrates, the state variable estimation was generally successful. Though the model and predicted lines do not perfectly overlap, the procedure estimates the overall shape of each parameter. It also pinpoints well the location of the Mikheyev–Smirnov–Wolfenstein (MSW) resonance. To hone this estimation even more, we will consider raising the maximum allowed β value and adjusting other factors like the search range and the value of R_f.

The parameter estimation as shown in Fig. 1b shows that the estimated value for p_a stabilizes around 11, while the true value is 13. While this match is not exact, it is a promising result because it is stable (after $\beta = 17$) and close to the true value. While failed runs tend to show the parameter estimation "fleeing" to the edges or midpoint of the search range, this run does not exhibit such behavior. We anticipate that as we are able to improve the state variable estimation, the parameter estimation value will improve as well.

5.2 Logistic Function for Electron Number Density

The second experiment involves our logistic model for $V(r)$ as described in Eq. 8 involves four parameters. In creating the model beams, we used the parameters specified in Sec. 4.2. For our optimization procedure, we consider single parameter estimation of the parameter L, which controls the height of function's upper asymptote. We applied a search range for L of $.001 - .02$ which is asymmetrical about the true value of $L = .049$. As was true for the exponential function experiment, the procedure terminated when $\beta = 25$.

Our results for one beam of this experiment are presented in Figure 2. Solutions for the state variables and $V(r)$ (labelled Vmatt in the figure) are plotted against the corresponding model values in Figure (2). This plot represents annealing iteration $\beta = 25$, which was the final iteration and thus the most accurate. As this figure illustrates, the optimization procedure's solution converges to the model for all three state variables as well as for $V(r)$. The accurate

prediction of $V(r)$ indicates the procedure successfully determined the correct value for the parameter L. In fact, the numerical solution for L was within 1.68×10^{-4}, or .36%, of the true value.

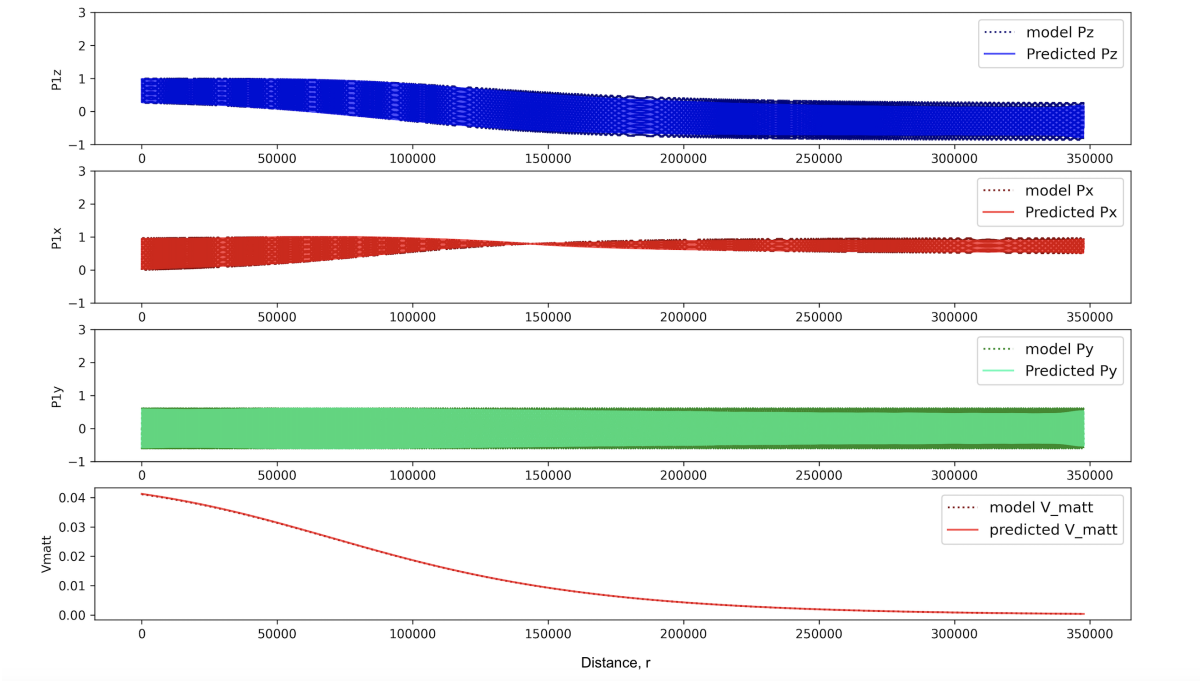

Figure 2: Results from the optimization procedure for a logistically decaying $V(r)$ model

While this result is extremely encouraging, it still uses significantly more measurement values than does the exponentially decaying $V(r)$ model.

Next steps will include adjusting search ranges, numbers of locations given, and determining any other factors that may affect the ability of the procedure to perform parameter estimation. Our first goal is to achieve parameter estimation using locations spaced along just the first and last 1000 points. The ultimate goal, as for the exponential case, is to successfully estimate parameters using only measurements toward the end of the trajectory. It remains unclear whether this goal is realistic or whether constraints will need to be put in place near the beginning of the trajectory to guide the optimization procedure toward the correct solution.

6 Conclusion

We illustrated that inference-based optimization is capable of performing parameter estimation on a simplified solar neutrino model. We implemented the optimization procedure on two different functional forms of the distribution of solar matter, $V(r)$, in each case successfully estimating the unknown parameter. Future efforts include attempting parameter estimation with fewer given measurements as well as introducing additional possible forms for $V(r)$. Additionally, we are working to introduce the Earth/Sun transformation, which connects the state variable P_z to measurable $P_{survival}$ values, so that we can utilize real data in our analysis.

Acknowledgements

Thanks to the NSF summer Research Experience for Undergraduates program for funding this research. I'd also like to thank Eve Armstrong, who mentored me this summer and helped me along every step of the research process, as well as the rest of the research team working on the

project: Mary Sanchez, Lily Newkirk, Carrie Laber-Smith, Hansen Torres, and Sara Rangiwala. Finally, I'd like to thank Eric Jones for helping me understand the optimization methodology.

References

[1] A. B. Balantekin, S. H. Fricke, and P. J. Hatchell. Analytical and semiclassical aspects of matter-enhanced neutrino oscillations. *Phys. Rev. D*, 38:935–943, Aug 1988.

[2] Huaiyu Duan, George M. Fuller, J. Carlson, and Yong-Zhong Qian. Simulation of coherent nonlinear neutrino flavor transformation in the supernova environment: Correlated neutrino trajectories. *Phys. Rev. D*, 74:105014, Nov 2006.

[3] H Duan, G M Fuller, and J Carlson. Simulating nonlinear neutrino flavor evolution. *Computational Science and Discovery*, 1(1):015007, nov 2008.

[4] Sherwood A. Richers, Gail C. McLaughlin, James P. Kneller, and Alexey Vlasenko. Neutrino quantum kinetics in compact objects. *Phys. Rev. D*, 99:123014, Jun 2019.

[5] Sherwood Richers, Don E. Willcox, Nicole M. Ford, and Andrew Myers. Particle-in-cell simulation of the neutrino fast flavor instability. *Phys. Rev. D*, 103:083013, Apr 2021.

[6] Sherwood Richers, Donald Willcox, and Nicole Ford. Neutrino fast flavor instability in three dimensions. *Phys. Rev. D*, 104:103023, Nov 2021.

[7] Chinami Kato, Hiroki Nagakura, and Taiki Morinaga. Neutrino transport with the monte carlo method. ii. quantum kinetic equations. *The Astrophysical Journal Supplement Series*, 257(2):55, dec 2021.

[8] Hiroki Nagakura. General-relativistic quantum-kinetics neutrino transport. *Phys. Rev. D*, 106:063011, Sep 2022.

[9] Manu George, Chun-Yu Lin, Meng-Ru Wu, Tony G. Liu, and Zewei Xiong. Cosev: A collective oscillation simulation engine for neutrinos. *Computer Physics Communications*, 283:108588, 2023.

[10] Irene Tamborra and Shashank Shalgar. New developments in flavor evolution of a dense neutrino gas. *Annual Review of Nuclear and Particle Science*, 71(1):165–188, 2021.

[11] Sherwood Richers and Manibrata Sen. Fast flavor transformations. In *Handbook of Nuclear Physics*, pages 1–17. Springer Nature Singapore, 2022.

[12] Eugenia Kalnay. *Atmospheric Modeling, Data Assimilation and Predictability.* Cambridge University Press, 2002.

[13] G. Evensen. *Data Assimilation: The Ensemble Kalman Filter*. Springer Science Business Media, 2009.

[14] William G. Whartenby, John C. Quinn, and Henry D. I. Abarbanel. The number of required observations in data assimilation for a shallow-water flow. *Monthly Weather Review*, 141(7):2502 – 2518, 2013.

[15] Z. An, D. Rey, J. Ye, and H. D. I. Abarbanel. Estimating the state of a geophysical system with sparse observations: time delay methods to achieve accurate initial states for prediction. *Nonlinear Processes in Geophysics*, 24(1):9–22, 2017.

[16] B.A. Toth, M. Kostuk, and C.D. Meliza et al. Dynamical estimation of neuron and network properties i: variational methods. *Biological Cybernetics*, 105:217–237, 2011.

[17] Eve Armstrong, Amol Patwardhan, Lucas Johns, Chad Kishimoto, Henry Abarbanel, and George Fuller. An optimization-based approach to neutrino flavor evolution. *Physical Review D*, 96, 12 2016.

[18] Eve Armstrong, Amol V. Patwardhan, A. A. Ahmetaj, M. Margarette Sanchez, Sophia Miskiewicz, Marcus Ibrahim, and Ishaan Singh. Inference of bipolar neutrino flavor oscillations near a core-collapse supernova based on multiple measurements at earth. *Phys. Rev. D*, 105:103003, May 2022.

[19] Caroline Laber-Smith, A. A. Ahmetaj, Eve Armstrong, A. Baha Balantekin, Amol V. Patwardhan, M. Margarette Sanchez, and Sherry Wong. Inference finds consistency between a neutrino flavor evolution model and earth-based solar neutrino measurements. *Phys. Rev. D*, 107:023013, Jan 2023.

[20] K. Hirata, T. Kajita, M. Koshiba, M. Nakahata, Y. Oyama, N. Sato, A. Suzuki, M. Takita, Y. Totsuka, T. Kifune, T. Suda, K. Takahashi, T. Tanimori, K. Miyano, M. Yamada, E. W. Beier, L. R. Feldscher, S. B. Kim, A. K. Mann, F. M. Newcomer, R. Van, W. Zhang, and B. G. Cortez. Observation of a neutrino burst from the supernova sn1987a. *Phys. Rev. Lett.*, 58:1490–1493, Apr 1987.

[21] R. M. Bionta, G. Blewitt, C. B. Bratton, D. Casper, A. Ciocio, R. Claus, B. Cortez, M. Crouch, S. T. Dye, S. Errede, G. W. Foster, W. Gajewski, K. S. Ganezer, M. Goldhaber, T. J. Haines, T. W. Jones, D. Kielczewska, W. R. Kropp, J. G. Learned, J. M. LoSecco, J. Matthews, R. Miller, M. S. Mudan, H. S. Park, L. R. Price, F. Reines, J. Schultz, S. Seidel, E. Shumard, D. Sinclair, H. W. Sobel, J. L. Stone, L. R. Sulak, R. Svoboda, G. Thornton, J. C. van der Velde, and C. Wuest. Observation of a neutrino burst in coincidence with supernova 1987a in the large magellanic cloud. *Phys. Rev. Lett.*, 58:1494–1496, Apr 1987.

[22] L. Wolfenstein. Neutrino oscillations in matter. *Phys. Rev. D*, 17:2369–2374, May 1978.

[23] A B Balantekin and H Yüksel. Global analysis of solar neutrino and kamland data. *Journal of Physics G: Nuclear and Particle Physics*, 29(4):665, mar 2003.

[24] Jingxin Ye, Daniel Rey, Nirag Kadakia, Michael Eldridge, Uriel I. Morone, Paul Rozdeba, Henry D. I. Abarbanel, and John C. Quinn. Systematic variational method for statistical nonlinear state and parameter estimation. *Phys. Rev. E*, 92:052901, Nov 2015.

[25] M. Agostini et al. Comprehensive measurement of pp-chain solar neutrinos. *Nature*, 562(7728):505–510, 2018.